Statistical Characterization, Modelling and Classification of Morphological Changes in imp Mutant Drosophila Gamma Neurons

Agustina Razetti, Xavier Descombes, Caroline Medioni, Florence Besse

Statistical Characterization, Modelling and Classification of Morphological Changes in *imp* Mutant Drosophila Gamma Neurons

Razetti A.[1], Descombes X.[2], Medioni C.[3], and Besse F.[3]
[1]*University of Nice Sophia Antipolis, I3S, 2000 Route des Lucioles, Sophia Antipolis, France*
[2]*Inria, CRISAM, 2003 Route des Lucioles, Sophia Antipolis, France*
[3] *Institute of Biology Valrose, University of Nice Sophia Antipolis, Parc Valrose, Nice, France*
arazetti@unice.fr, xavier.descombes@inria.fr, {caroline.medioni, florence.besse}@unice.fr

Keywords: Gamma neurons, Remodelling, Stochastic models, Likelihood analysis.

Abstract: In Drosophila brain, gamma neurons in the mushroom body are involved in higher functions such as olfactory learning and memory. During metamorphosis, they undergo remodelling after which they adopt their adult shape. Some mutations alter remodelling and therefore neuronal final morphology, causing behavioural dysfunctions. The RNA binding protein Imp, for example, was shown to control this remodelling process at least partly by regulating *profilin* expression. This work aims at precisely characterizing the morphological changes observed upon imp knockdown in order to further understand the role of this protein. We develop a methodological framework that consists in the selection of relevant morphological features, their modelling and parameter estimation. We thus perform a statistical comparison and a likelihood analysis to quantify similarities and differences between wild type and mutated neurons. We show that *imp* mutant neurons can be classified into two phenotypic groups (called Imp L and Imp Sh) that differ in several morphological aspects. We also demonstrate that, although Imp L and wild-type neurons show similarities, branch length distribution is discriminant between these populations. Finally, we study biological samples in which Profilin was reintroduced in *imp* mutant neurons, and show that defects in main axon and branch lengths are partially suppressed.

1 INTRODUCTION

Gamma neurons in *Drosophila* brain mushroom body are in charge of high functions such as olfactory learning and memory (Xie et al., 2013). Mutations affecting their adult shape cause several behavioural dysfunctions (Redt-Clouet et al., 2012).

During metamorphosis, gamma neurons go through a process of pruning –where the main part of their axons and dendrites is lost– followed by regrowth, resulting in the establishment of the adult shape (Williams and Truman, 2005). The understanding of this process and its main involved factors is critical to explain why some mutations cause important changes in the neuron adult morphology.

This study is focused on the remodelling process, composed by regrowth and branching after pruning. The correct development of this process gives rise to well-formed and functional adult neurons.

Medioni et al. (2014) have shown that the RNA binding protein Imp is not essential during the initial axonal growth of gamma neurons, but is necessary during their remodelling. This work shows that, in adults, ~50% of *imp* mutants display shorter axons than wild types (WT) and fail to reach their target. Imp mutants also exhibit an overall loss of branch number and complexity. Molecular and genetic analysis have further shown that *profilin* mRNA, which encodes an actin cytoskeleton regulator (Verheyen and Cooley, 1994), is a direct and functional target of Imp and both are key regulators of the Drosophila gamma neuron axonal remodelling process, acting on the same molecular pathway. Interestingly, the overexpression of *profilin* in imp mutants partially rescues the main axon length, but not the branch complexity (Figure 1). These results suggest that Imp controls axonal extension during remodelling by regulating *profilin* mRNA expression. However they also suggest that the branching process may be dependent on the regulation of other Imp mRNA targets, yet to be identified.

In this paper, we intend to further understand the role of Imp and the importance of *profilin* mRNA

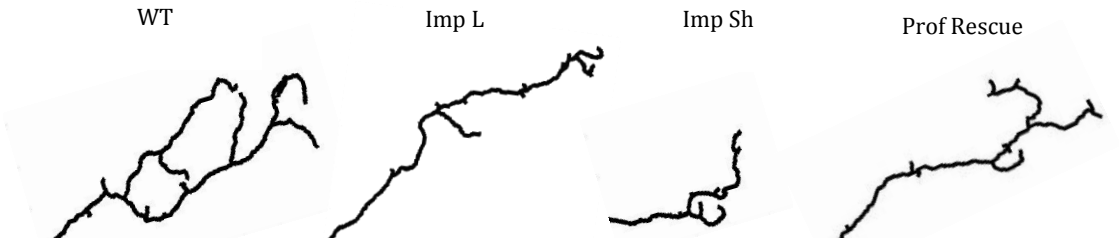

Figure 1: Representation of the morphology of each one of the groups under study (in order: Wild type, *imp* mutant and *imp* mutant rescued by Profilin). *imp* mutants are divided into short and long species (named Imp Sh and Imp L respectively) as both phenotypes are equally observed (Medioni et al., 2014).

expression regulation during remodelling by deeply analysing the impact of Imp knockdown in neuron development. To overcome the variability of axonal projection patterns associated with a given biological sample, we propose to identify the main features of adult gamma neuron morphology and quantify their similarities and differences between WT and mutated axons using a well-defined statistical framework. This approach provides both a biological interpretation and a quantification of resemblance between biological samples. This framework is general and can be applied to model and characterize neuron types.

Because effects of Imp knockdown and rescue with Profilin can be identified in the main axon as well as in the branch development or independently, we consider both structures separately. The four features we chose are: "main axon length", "main axon shape", "first order branch distribution along the main axon" and "branch length distribution". To measure these features, we segmented a set of images corresponding to each neuron type to obtain a numeric tree-shaped skeleton representing the morphology of each neuron. We then measured the features values using homemade software. The image segmentation as well as the measurement of each feature are described in the following sections.

Neuron morphological automatic classification has already been addressed in the bibliography. Kong et al. (2005) proposed an unsupervised clustering of ganglion cells in the mouse retina by the k-means algorithm in order to define cell types. They initially disposed of 26 morphological parameters and found out that clustering with only three of them was the most effective way. Guerra et al. (2011) establish the advantage of applying supervised classification methods regarding morphological feature based classification to distinguish between interneurons and pyramidal cells. They also conclude that reducing the number of features to an optimal number outperforms the classical approach of using all the available information. Lopez-Cruz et al. (2014) built a consensus Bayesian multinet representing the opinions of a set of experts regarding the classification of a pool of neurons. The morphological parameters chosen by each expert to make their decisions are not considered. A different approach was proposed by Mottini et al. (2014) which consists on classifying different neuron types by reducing them to trees and calculating a distance, combining geometrical and topological information.

Nevertheless, the different published approaches intend to accurately discriminate between different types of neurons, considering misclassification as a methodological error and consequently developing techniques to avoid these cases. However, similarities between populations are not necessarily to be excluded as they may reflect the properties of biological samples and help us in their characterization. Furthermore, these methods do not intend to understand which morphological characteristic is discriminant between different species. A deeper multi-criteria statistical analysis is thus required. Our approach thus consists in developing a probabilistic model for each of the mentioned features and estimate the associated parameters. The similarities or dissimilarities between the populations for each feature are assessed through statistical tests under null hypothesis and likelihood classification.

In the next section, we introduce each one of the features followed by the correspondent model. Next we present the results of the classification combining different criteria which allows to finally deduce the morphological changes induced by the studied mutations.

2 DATA

2.1 Images

We used 3D images taken with a confocal microscope. Each set of images show the distal part of an axonal tree at adult stage (Figure 2). Single axons are labelled by GFP using the MARCM technique (Wu and Luo, 2006), which allows to image a single mutated (or wild type) neuron in a wild type environment. The database we used for this study consists of 46 wild type images, 48 *imp* mutants and 15 *imp* mutants rescued by Profilin.

The voxel size varies among the images and is anisotropic in the Z axis. The voxel length in Z is between 5 and 12 times its length in X and Y, which varies from 0.09 to 0.15 µm.

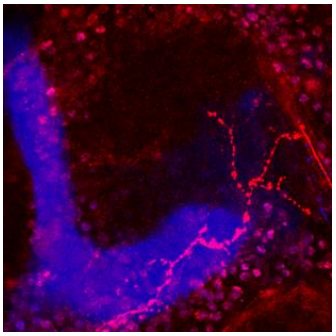

Figure 2: Maximum intensity Z projection showing a wild type axon (red) and the morphology of the mushroom body (blue).

2.2 Segmentation

To avoid artificial jumps along the Z axis due to image anisotropy, we applied a simple quadratic interpolation algorithm included in FIJI (the open source image analysis software developed by NIH, Maryland, USA) (Schindelin et al., 2012).

An automatic segmentation of the images is still not available in our case due to noisy background and poorly defined neuron trace. When observing the images, it can be not trivial even for experts to determine the correct 3D path followed by main axons and their branches. Their trajectories can be very complex as well as non-continuous and difficult to differentiate from background structures. Therefore we segmented the images with the open software Neuromantic (Myatt et al., 2012), specially developed to segment 2 or 3D neurons manually or semi-automatically. As output we obtain a set of points along the main axon and branches that we connect using a Bresenham-inspired 6-connectivity algorithm. We chose this connectivity to keep further measurements and models simple. After this process we obtain a tree-like set of numeric 3D curves that describe the morphology of each neuron (Figure 3).

To ensure all the neurons to be similarly oriented we rotated the images to align the medial and the dorsal lobes with the X (horizontal) and Y (vertical) axis correspondingly. The beginning of each neuron was considered just before entering the medial lobe. No further registration was applied to the images, to avoid axon deformation. Conserved morphology was preferred rather than more accurate spatial location.

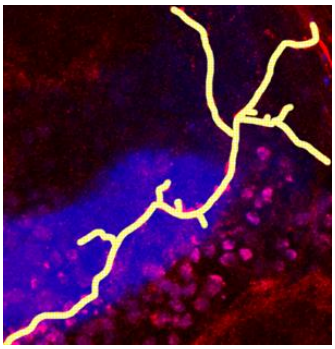

Figure 3: Detail of the Z projected image showed in Figure 2, where the neuron has been segmented (yellow) to obtain a tree-like set of numeric 3D curves.

2.3 Tree hierarchy

When studying their morphology it is necessary to understand how neurons are structured i.e. main axon and first, second, third (etc.) order branches (the neuron body and dendrites are not present in the studied images). To accurately label the paths forming the tree that represents each neuron, we have developed an automatic pseudo-recursive algorithm capable of processing trees of any order. It first takes the whole tree and labels the selected path as the main axon, followed by a repeated identical analysis of all the resulting sub-trees. In each step, the main path is assigned following the criteria used by experts when done visually: total length, directionality and sense coherence. To achieve this, in each step we consider the points in all the paths between the root and the leaves of the tree (i.e. the whole axon) or subtree and calculate their linear regression obtaining a straight guideline, which will determine directionality and sense coherence. For each path in the analysed subtree, a cost function is computed that depends on the distance between each point in the path and the guideline (directionality), the parallelism between them (accounting for the sense coherence) and the path total length. Finally the path that minimizes this cost function is selected as main axon in the case of the whole tree (first step), or main branch in the case of the different subtrees (Figure 4).

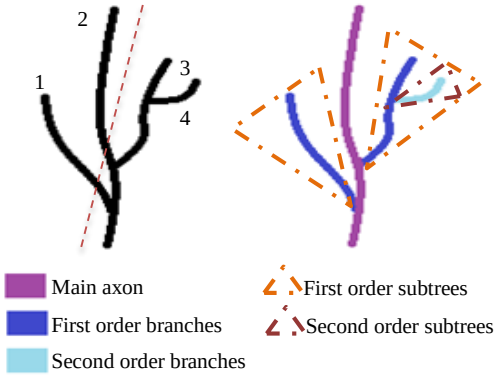

Figure 4: Scheme of the three-hierarchy algorithm. For a given tree, the guideline is calculated followed by the cost function for each possible path (1-4). The one that minimizes it is assigned as main axon (here path 2). The algorithm is applied recursively to each subtree resulting in the hierarchy of the entire tree.

3 MODEL DEVELOPMENT

After the segmentation, interpolation in the Z axis and tree hierarchy algorithm, the neuron skeletons become a 3D tree made out of unitary segments described by their round coordinates or pixels. Taking this simple neuron geometrical description into account, we define the main features that describe and discriminate the individuals under study: the main axon length and sinuosity, as well as the branch density and length distribution. In the following sections we describe the probabilistic models for each feature and compute associated statistical tests under null hypothesis between the different groups (WT: wild type neurons that are used as controls, Imp: neurons with *imp* knockdown, reported to be morphologically aberrant in the literature, and Prof Rescue: *imp* mutants with an overexpression of *profilin*, known to partially suppress the *imp* phenotype). Besides, we derive the likelihood of each model.

3.1 Main axon length

The main axon length was measured taking the total amount of pixels in the corresponding path and multiplying by the pixel size (µm). The length distribution was modelled as Gaussian where the mean and standard deviation for each group ($\mu_{m.a.}$, $\sigma_{m.a.}$) were calculated from data. We observed the bimodal behaviour in the Imp group reported by Medioni et al. (2014) (Figure 5). Therefore, to make a more accurate modelling of this parameter, we separated Imp mutant neurons into two groups - neurons with long axons (Imp L) and neurons with short axons (Imp Sh)- using the k-means algorithm. 54% of the neurons were assigned to Imp Sh and 46% to Imp L, consistent with the percentage reported by Medioni et al. (2014). Figure 5 shows the main axon length histograms for each group, Imp divided into Imp L and Imp Sh.

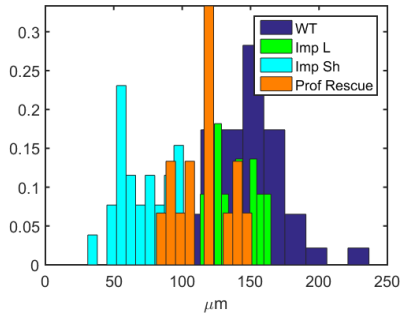

Figure 5: Main axon length distributions for each biological sample.

To know which groups can be considered to present significantly different main axon length measurements, non-parametric Kruskal Wallis tests were carried out between all the possible pairs of groups (Table 1). We chose this test for the sake of consistency, as it can be applied to analyse all the features (independently of each model). For *p* values inferior to 5%, we consider that the null hypothesis that both distributions are the same can be rejected. Thus, the only pair not presenting a significant difference is WT and Imp L. It is relevant to highlight that Prof Rescue distribution lies in between the distributions for Imp L and Sh and even though more similar to Imp L, still significantly different.

Table 1: *p* values from the non-parametric Kruskal Wallis test comparing the main axon length between the studied groups.

	Imp L	Imp Sh	Prof Rescue
WT	0.1219	5.0098E-12	0.000144
Imp L		3.2627E-09	0.0013
Imp Sh			2.48E-06

The likelihood of a given neuron *n* of length l_n to belong to a given group is defined by the Normal probability density function

$$L_l(l_n|n \in X) = P(l_n|n \in X)$$

$$= \frac{1}{\sigma^X_{m.a}\sqrt{2\pi}} e^{\frac{-(l_n-\mu^X_{m.a})^2}{2\sigma^{X\ 2}_{m.a}}}, \quad (1)$$

where $(\mu^X_{m.a}, \sigma^X_{m.a})$ are the mean and standard deviation of the main axon length corresponding to the group *X*.

3.2 Main axon morphology

To define the shape model, we consider as random variable the unit vector $\vec{x}_t$ that accounts for the shift of the axon tip between *t-1* and *t*. Because we consider the 6-connectivity and backwards moves are not allowed, each $\vec{x}_{t+1}$ can take five different values, as shown in Figure 6. Assuming the main axon development follows a second order Markov property, we have

$$P(\vec{x}_{t+1}|\, \vec{x}_i\ i \le t) = P(\vec{x}_{t+1}|\, \vec{x}_t, \vec{x}_{t-1}). \quad (2)$$

The morphology model is then completely defined by the conditional probabilities $P(\vec{x}_{t+1}|\, \vec{x}_t, \vec{x}_{t-1})$. There are 30 possible combinations of the two unit vectors $[\vec{x}_t,\ \vec{x}_{t-1}]$ and each of these combinations has five possible future jumps $\vec{x}_{t+1}$, giving a total of 150 possible transitions in *t+1*, each of them with probability P_i (conditionally to $[\vec{x}_t,\ \vec{x}_{t-1}]$). The order of the Markov chain was chosen to combine a discriminative efficiency between similarly shaped axons and a reasonable combinatorial to robustly estimate the conditional probabilities.

Figure 6 presents two basic configurations of a pair of unit vectors $[\vec{x}_t,\ \vec{x}_{t-1}]$ and their corresponding five possible $\vec{x}_{t+1}$. The one on the left depicts one of the six possible cases where the vectors $\vec{x}_t$ and $\vec{x}_{t-1}$ are in line (in this case in the +z direction). The second configuration exemplifies the 24 cases where the vectors $\vec{x}_t$ and $\vec{x}_{t-1}$ are not in line.

We estimate the conditional probabilities from data using the empirical estimator (3), where $\#_n$ accounts for the number of times the nth configuration of three unit vectors $[\vec{x}_{t+1},\ \vec{x}_t,\ \vec{x}_{t-1}]$ appears.

$$P_{5s+j} = \frac{\#_{5s+j}}{\sum_{k=1}^{5} \#_{5s+k}}, \begin{matrix} j = 1,\dots,5 \\ s = 0,\dots,29 \end{matrix} \quad (3)$$

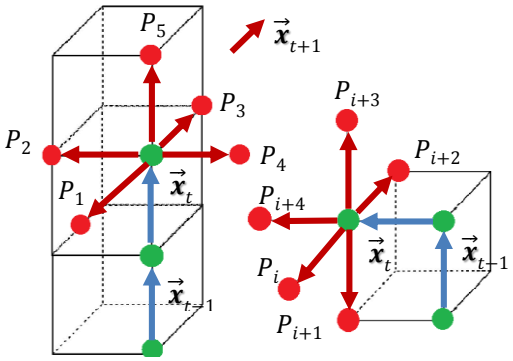

Figure 6: Two examples of three vector (past, present and future steps) configurations on a 3D 6-connected path. Each future direction has a probability of occurrence conditioned by the present and past directions and is numbered from 1 to 150.

We performed the Kruskal Wallis non-parametric test between populations for each P_i, $1 \le i \le 150$. Table 2 shows the amount of parameters P_i that presents a p value inferior to 5% between each pair of populations.

Table 2: Number of parameters with p<0.05 for the non-parametric Kruskal Wallis test.

	Imp L	Imp Sh	Prof Rescue
WT	12	22	28
Imp L		16	19
Imp Sh			14

Regarding the possible two past unit vectors $[\vec{x}_t,\ \vec{x}_{t-1}]$, the results of the estimation show that all the groups share the six most frequent configurations, representing together between 65 and 76% of the total.

The computation of the Markov chain likelihood appears to lack of robustness when comparing populations. This can be explained by the limited length of the axons in pixels (~1500) and the combinatorial of the problem (150 conditional probabilities). Indeed, some of the three vector configurations, even though with non-zero probability, may not appear in the learning sample. When this is the case, if the axon to classify does present at least one time this configuration the likelihood becomes zero. This means that the likelihood is extremely sensible to fluctuations in the presence of low probable events, which is statistically inevitable with the size of our data. To overcome this inconvenience and add robustness to the likelihood analysis, we consider the 30 probability distributions $P(\vec{x}_{t+1}|\, \vec{x}_t, \vec{x}_{t-1})$ as independent, and define a

multinomial Bernoulli distribution for each possible value of $\vec{x}_{t+1}$ given $[\vec{x}_t,\ \vec{x}_{t-1}]$.

For each neuron *n*, the likelihood of each group *X* according to the shape model of *X*, $P_{i,X}$, and the frequencies of appearance of three unit vectors corresponding to *n*, $\#_i$, is then defined as follows

$$
\begin{aligned}
&L_{sh}(\#_1 - \#_{150} | n \in X) \\
&= P(\#_1 - \#_{150} | n \in X) \\
&= \prod_{s=0}^{29} P\left(P_{5s+1} - P_{5s+5} | n \in \mathrm{X} \right) = \\
&\prod_{s=1}^{30} \left(\binom{N_s}{\#_{k+1}} P_{k+1}{}^{\#_{k+1}} \binom{N_s - \#_{k+1}}{\#_{k+2}} P_{k+2}{}^{\#_{k+2}} \right. \\
&\binom{N_s - \#_{k+1} - \#_{k+2}}{\#_{k+3}} P_{k+3}{}^{\#_{k+3}} \\
&\binom{N_s - \#_{k+1} - \#_{k+2} - \#_{k+3}}{\#_{k+4}} P_{k+4}{}^{\#_{k+4}} \\
&\left. P_{k+4}{}^{\#_{k+5}} \right).
\end{aligned}
\tag{4}
$$

$$
k = 5(s-1), \qquad N_s = \sum_{j=1}^{5} \#_{5(s-1)+j}
$$

3.3 Branch density

We propose a model to describe the branching point distribution independently of the axon length, based on the biological process of interstitial branch formation during development. This process can be described in three simple steps (Figure 7): A. the main axon grows following particular external and internal guiding cues. B. When the growth cone senses external guiding cues indicating the formation of an interstitial branch, the main axon decreases its growing speed until it stops while it accumulates molecular material in its tip. C. After some time the main axon continues growing following its particular cues, leaving the accumulated material in a specific zone of its shaft. The left material has been organized into an independent growing tip and starts elongating an interstitial branch towards its particular target, different from the one of the main axon (Szebenyi et al., 1998).

In summary, the emergence of an interstitial branch depends on the presence of specific external guiding cues that cause the modification of the axon growing rate, which allows the accumulation of the molecular material needed for the creation of the new branch. Modelling this process becomes initially unreachable as none of this two features (growing rate, guiding cues presence) can be measured from the adult stage static images available as data. Regarding this limitations, we propose a model to mimic this dynamic process from our static data. We focus our study on the behaviour of the axon growing rate, starting with a certain initial speed v_o and evolving until $v = 0$, when a new branch point appears.

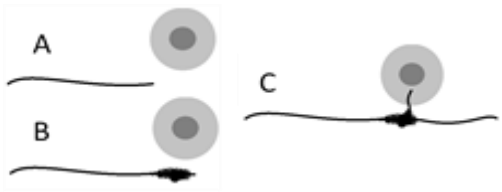

Figure 7: Interstitial branch formation during axonal development described schematically in three main steps, adapted from Szebenyi et al. (1998).

We can measure the number *k* of pixels between every two successive branching points along the main axon of a segmented neuron. Then we suppose that each one of this pixels represents a differential progress in the axonal growth where, during development, the axon had a certain growing rate v. Our model assumes random decreases in speed which we call Δv, with a probability of occurrence *p*. When a certain number of decreases Δv occur, the speed v equals zero thus the growing tip stops, allowing the material needed to form a branch to accumulate. After some time the process starts again, with initial speed v_o.

Because at each one of the *k* pixels a decrease in v may or not happen, we describe the problem using a Bernoulli probability distribution (Forbes et al., 2011) where each success means a differential decrease in speed. We consider that the growing rate goes to zero after *A*+1 steps of speed decreasing. The probability to reach $v = 0$ after *k* steps is then written as follows:

$$
P(k) = \binom{k-1}{A} p^{A+1} (1-p)^{k-A-1} . \tag{5}
$$

Equation (5) gives the probability of having *A* successes in $k-1$ trials and a success in the k^{th} trial. This means the axon tip decreases its speed *A* times before stopping completely (which happens in *A*+1), or equivalently that the length between two branching points is *k* (Figure 8). Thus, our Bernoulli-based, time-mimicking branching point distribution model has two parameters, *A* and *p*, to be estimated from data. Knowing the distances *k* between successive

branching points for every axon in each group, we can calculate their mean and variance μ_k and $\sigma^2{}_k$. From

$$\mu_k = \sum_i k_i \binom{k_i - 1}{A} p^{A+1}(1-p)^{k_i - A - 1} \quad (6)$$

and

$$\sigma^2{}_k = \sum_i k_i{}^2 \binom{k_i - 1}{A} p^{A+1}(1-p)^{k_i - A - 1} - \mu_k{}^2 \quad (7)$$

it can be shown that $\mu_k(A,p)$ and $\sigma^2{}_k(A,p)$ have the simple forms

$$\mu_k(A,p) = \frac{A}{p}, \qquad \sigma^2{}_k(A,p) = \frac{(1-p)A}{p^2} \quad (8)$$

which allow to easily estimate A and p from data. Once A and p are estimated, A needs to be rounded as it has to be an integer. Then p can be recalculated knowing the value of A as

$$p = \frac{\sqrt{A(\mu_k + \sigma^2{}_k)}}{\mu_k + \sigma^2{}_k}. \quad (9)$$

The number A+1 of needed accumulation of increments Δt_i and p their probability to happen will define each axonal group regarding their branch density.

Table 3 and Table 4 present the resulting values of A and p for each group and the p values from the non-parametric Kruskal Wallis test of the distances between two consecutive branches k among neuron groups, respectively.

While every group has the same value of A, Imp Sh presents the highest value of p meaning that Δv occurrence is more probable and it takes less time to reach $v = 0$, thus it is the most branched group. This difference is significant ($p<0.05$) between Imp Sh and every other group.

To calculate the likelihood of each neuron n to belong to the group X regarding this model, we use the Binomial probability density function considering the distances between each pair of branches $k_{n,m}$ independent between them, obtaining

$$L_{bp}(k_{n,m}|n \in \mathrm{X}) = P(k_n = \{k_{n,1}, \dots, k_{n,M}\}|n \in \mathrm{X}) = \prod_{\mathrm{m}=1}^{\mathrm{M}} P(k_{n,m}|n \in \mathrm{X}) = \prod_{\mathrm{m}=1}^{\mathrm{M}} \binom{k_{n,m} - 1}{A_X} p_X{}^{A_X+1} p^{k_{n,m}-1-A_X} \quad (10)$$

where M is the total number of pairs of branches.

Figure 8: 2D 4-connected path showing the axonal trajectory until the formation of a branching point (3D not shown for simplicity). Pink pixels occur with a probability p, decreasing the growing rate. When the number of pink pixels equals A+1, v_i=0 and a new branching point appears.

Table 3: p values from the non-parametric Kruskal Wallis test comparing the distances in pixels between consecutive branches between the studied groups.

	Imp L	Imp Sh	Prof Rescue
WT	0.9398	4.20E-03	0.5704
Imp L		2.16E-02	0.6478
Imp Sh			1.32E-02

Table 4: Value of the parameters A and p describing the branching points distribution.

	A	p	p for A=1
WT	1.2	0.0087	0.0078
Imp L	1.0	0.0068	0.0067
Imp Sh	0.9	0.008	0.0084
Prof Rescue	1.2	0.0074	0.0068

3.4 Branch length distribution

To study the branch length distribution within the neuron groups, we established four length categories (μm); L_1: (0,1], L_2: (1,5], L_3: (5,10] and L_4: (10, ∞)

following Tessier and Broadie (2008). The length was measured in the same way as described for the main axon, and branches of all levels were taken into account. For each group of axons we calculated the mean and standard deviation (μ_{bi}, σ_{bi}), $1<i<4$ of the relative number of branches corresponding to each length category per axon b_1-b_4 (i.e. number of branches in each length category normalized by the total number of branches, per axon).

The percentage of branches in each category is shown in Table 5.

Table 5: Branch length distribution by length and neuron group (%).

	L_1	L_2	L_3	L_4
WT	10.6	49.2	11.7	28.5
Imp L	8.4	66.5	10.1	15
Imp Sh	19.8	48.2	14.5	17.5
Prof Rescue	19.5	48.3	10.2	22

To know between which groups and length category the differences in the results displayed in Table 5 are significant we performed the Kruskal Wallis non-parametric test for the four length groups. Significant results ($p<0.05$) are only present in L_2 and L_4. The p values are shown in Table 6 and Table 7.

Table 6: p values from the non-parametric Kruskal Wallis test comparing the branch length distribution in L_2 between the studied groups.

L_2	Imp L	Imp Sh	Prof Rescue
WT	8.92E-05	0.9392	0.7884
Imp L		9.04E-04	0.0014
Imp Sh			0.9134

Table 7: p values from the non-parametric Kruskal Wallis test comparing the branch length distribution in L_4 between the studied groups.

L_4	Imp L	Imp Sh	Prof Rescue
WT	3.45E-04	1.29E-04	0.1822
Imp L		0.7383	0.1238
Imp Sh			0.1387

Imp L presents significantly more branches in L_2 than any other group while WT has a bigger proportion of L_4 branches than Imp L and Sh, but not Prof Rescue. For further analysis we take the categories L_2 and L_4.The distribution modelling the relative amount of branches within these length categories and for each group was considered as Gaussian.

To calculate the likelihood of each neuron n with each group X regarding the branch length distribution in L_2 and L_4 -$b_{n,2}$ and $b_{n,4}$- we considered a bivariate Gaussian distribution with mean $\vec{\mu}_b^X = (\mu_{b2}^X, \mu_{b4}^X)$ and Σ^X the covariance matrix between b_2^n and b_4^n.

$$L_{bl}(\vec{b}_n | n \in \mathrm{X}) = P(\vec{b}_n | n \in \mathrm{X}) = \frac{1}{2\pi\sqrt{|\Sigma^X|}} e^{-\frac{1}{2}(\vec{b}_n - \vec{\mu}_b^X)^T \Sigma^{X^{-1}} (\vec{b}_n - \vec{\mu}_b^X)}, \quad (11)$$

where $|\Sigma^X|$ is the determinant of the covariance matrix Σ^X.

4 LIKELIHOOD ANALYSIS

For a neuron n, we calculate the corresponding features and then compute the likelihood for each group of neurons X, ($\mathrm{X} \in \{\mathrm{WT}, \mathrm{Imp}, \mathrm{Prof\ Rescue}\}$). The neuron n is then classified in the group that maximizes the global likelihood. All the classifications present in this work were done using the *leave one out* technique, which consists in classifying a sample that has been removed from the database to perform the learning stage, i.e. the estimation of the distribution parameters. This maximum likelihood classification provides some assessment about the discriminative properties of the proposed models but is also used to analyse the mixture of feature values between the populations.

Considering our four features to be independent from each other, the global likelihood is given as follows

$$L(\{l_n, \#_{1,n} - \#_{150,n}, k_n, \vec{b}_n\} | n \in \mathrm{X}) = L_l(l_n | n \in \mathrm{X}) L_{sh}(\#_{1,n} - \#_{150,n} | n \in \mathrm{X}) \, L_{bp}(k_n | n \in \mathrm{X}) L_{bl}(\vec{b}_n | n \in \mathrm{X}), \quad (12)$$

and the maximum likelihood estimation results

$$n \in \mathrm{X}_o \leftrightarrow \mathrm{X}_o = \underset{\mathrm{X}}{\operatorname{argmax}} L(\{l_n, \#_{1,n} - \#_{150,n}, k_n, \vec{b}_n\} | n \in \mathrm{X}) \quad (13)$$

$$\mathrm{X} = \{\mathrm{WT}, \mathrm{Imp\ L}, \mathrm{Imp\ Sh}, \mathrm{Prof\ Rescue}\}.$$

Equation (13) allows to classify each neuron by resemblance to each group considering the four morphological features and their mathematical models. Table 8 presents the results of the general resemblance analysis.

Table 8: General likelihood analysis considering the four features. Imp L and Imp Sh reconsidered separately.

		Predicted (%)		
		WT	Imp L	Imp Sh
Actual Class	WT	82.6	17.4	0
	Imp L	54.5	45.5	0
	Imp Sh	19.2	3.9	76.9

This results suggest a relevant difference between neurons belonging to Imp L and Imp Sh, as well as between WT and Imp Sh. More than half of Imp L are likely to be WT while for Imp Sh this propotion is less than 20%.

To understand how each morphological feature contributes to the results in Table 8, we carried out the likelihood analysis regarding each of them separately. For the main axon length, as expected from Figure 5, WT neurons are shared between WT and Imp L; and Imp L is correspondingly mixed with WT. Imp Sh is completely separated from the rest of the groups (Table 9).

Table 9: Likelihood analysis according to main axon length.

L		Predicted (%)		
		WT	Imp L	Imp Sh
Actual Class	WT	39.1	54.4	6.5
	Imp L	22.7	77.3	0
	Imp Sh	0	0	100

According to the main axon shape in Table 10, WT and Imp L look again similar and, interestingly, Imp Sh looks more similar to WT than to Imp L.

Table 10: Likelihood analysis according main axon shape.

SH		Predicted (%)		
		WT	Imp L	Imp Sh
Actual Class	WT	54.3	43.5	2.2
	Imp L	50	50	0
	Imp Sh	61.5	38.5	0

Table 11 presents the likelihood analysis results regarding the branch point density. It can be noticed that every group is mainly classified as Imp Sh, which our previous analysis revealed as the most branched group. The reason for this behaviour relies on the nature of the model. Even though the means of the distances between branches are different between the biological groups, axons frequently display one or more pairs of branches which are close. Because for close branches the likelihood is maximum for Imp Sh, with a significant difference from the other groups, the presence of near branches automatically classifies a neuron as Imp Sh. Nevertheless, the branch density coherence is respected for each group as the resemblance with Imp Sh is maximum for the most branched group (itself) and is followed in the correct order: WT and then Imp L.

Table 11: Likelihood analysis according branching point.

BP		Predicted (%)		
		WT	Imp L	Imp Sh
Actual Class	WT	0	13	87
	Imp L	13.6	18.2	68.2
	Imp Sh	7.7	11.5	80.8

Finally, according to the branch length distribution (Table 12) WT, Imp L and Imp Sh show a higher likelihood to their own groups, suggesting a significant difference between them regarding this feature.

Table 12: Likelihood analysis according branch length distribution.

BL		Predicted (%)		
		WT	Imp L	Imp Sh
Actual Class	WT	60.9	23.9	15.2
	Imp L	18.2	72.7	9.1
	Imp Sh	15.4	30.8	53.8

In order to analyse the morphological changes induced by profilin recue, we performed the general likelihood analysis considering either *imp* mutants altogether (Table 13), or split between Imp L and Imp Sh (Table 14). We have already shown in the previous section that Prof Rescue presents i) an histogram in between that one of Imp L and Imp Sh regarding the main axon length, ii) no significant difference with WT nor Imp L (but with Imp Sh) regarding branching point density and ii) it is the only group to present no

significant differences with WT regarding the branching length distribution.

Table 13: General likelihood analysis considering the four features. Prof. Rescue is included.

		Predicted (%)	
		WT	Imp
Actual Class	WT	80.4	19.6
	Imp	37.5	62.5
	Prof Rescue	60	40

Table 14: General likelihood analysis considering the four features. Imp L and Imp Sh reconsidered separately and Prof. Rescue is included.

		Predicted (%)		
		WT	Imp L	Imp Sh
Actual Class	WT	82.6	17.4	0
	Imp	35.5	23	41.5
	Prof Rescue	40	26.7	33.3

From the analysis in Table 13 we can highlight that while only 37.5% of *imp* mutants present a WT phenotype, the 60% of Profilin rescue neurons exhibit this behaviour. A deeper study, considering the subdivision of *imp* mutants in Imp Sh and Imp L (Table 14), shows that 40% of neurons in Prof Rescue present WT phenotype compared to 35% for Imp. Moreover, it is interesting to analyse how Prof Rescue is classified regarding Imp L and Imp Sh. The percentage of neurons classified as Imp Sh decreases compared to *imp* mutants from 41 to 33% while the tendency for Imp L is inversed, with 23% for Imp and 27% for Prof Rescue. We have also performed the likelihood analysis for Prof Rescue considering each feature separately, and observed that Prof Rescue presents 33% of short main axons compared to 54% in *imp* mutants, and a likelihood towards WT regarding the branch length distribution of 33%, which is around two times that of Imp L and Imp Sh.

Finally a brief comparison can be done regarding the classification results with those in Mottini et al. (2013), who analysed wild type as well as *imp* mutated gamma neurons. The authors report an 80.4 and 91.7% of accurate classifications for WT and *imp* mutants respectively with the ESA curve distance method and 85 and 79.2% with RTED. It is relevant to highlight that the goal in their work is to merely discriminate between populations, thus they privilege to consider exclusively highly discriminative parameters. On the contrary, our results -80.4 and 62.5% for WT and Imp respectively- aim to show and value not only the differences but also the existing similarities between phenotypes, considering relevant morphological features and link the conclusions with biological parameters. Finally, our sample size doubles the one used in the cited work.

5 DISCUSSION

5.1 Axon growing rate and branch formation

The value of A=1 indicates that the axon tip diminishes its growing speed only two times before stopping to create a branch, instead of doing it gradually. The first time can be related to when it senses the external guiding cues. Then it continues growing more slowly, which may facilitate other cues detection, until it finally stops, consequence of the second and last speed lost. When this happens, branching material is accumulated and after some time an interstitial branch is created. An increased value of p may indicate a higher sensibility to external cues as well as the presence of aberrantly stronger internal cues triggering branching. Another interpretation can be that axons with a defective growing rate (i.e. slower speed, or high p) are more susceptible to stop independently from external cues, and therefore to branch more.

All the groups present the same value of A indicating this two-step behaviour may be conserved and therefore independent from Imp. Regarding p, Imp Sh is significantly more branched than the rest of the groups, including Imp L, even though they have the same genotype. We suggest a correlation between the size of the main axon and the branch density for *imp* mutants. More interestingly, Profilin rescue axons present the same value of p than Imp L. This suggests that the phenotype presenting an aberrant branch density is rescued by *profilin* overexpression (or, in other words, is back to wild type branch density).

5.2 Wild type neurons are characterized by their branch length distribution

The general likelihood analysis results in more than 80% of WT axons to be correctly classified (Table 8, Table 13 and Table 14). Nevertheless, when looking at each particular feature it becomes evident that WT shares most of them with Imp L. Regarding the main

axon length (Table 9), 54% of WT neurons are likely to be Imp L and 43% for the main axon shape (Table 10). The analysis following the branching point density results in 13% of WT neurons likely to be Imp L, while no WT neuron was correctly classified. This results are validated by the *p* values for main axon length and branch length distribution that do not show significant differences. We encounter a similar situation regarding the shape model, as between Imp L and WT the amount of significantly different parameters is the minimum of all the group pairs and it is only 12 in 150.

Regarding the likelihood analysis taking branch length distribution, WT is well defined (Table 12). WT and Imp L present both 80% of branches in L_2 and L_4 (Table 5), with the difference that WT shows statistically more branches in L_4 while Imp L in L_2. We can relate our results to those of Tessier and Broadie (2008) and Medioni et al. (2014). The first publication reports that a loss of L_2 branches by a late pruning process occurs in wild type neurons and not in dFMRP mutants (dFMRP is also a profiling regulator) and the second one concludes a defective development of long branches (L_4) in *imp* mutants.

The maximal percentage of correct classification for WT considering the features separately is 60% for the branch length distribution (Table 12), followed by 54, 39 and even 0% corresponding to main axon shape, length and branching point distribution (Table 10, Table 9 and Table 11). Interestingly, the general classification mixing the four features improves these percentages up to 80% (Table 8, Table 13 and Table 14). This suggests that WT neurons are well defined and different from Imp mutants but it is necessary to consider all the morphological features together. This highlights the advantages of our method as it goes beyond a simple statistical analysis, allowing to mix different features as well as to consider each neuron independently.

5.3 *imp* knockdown presents two different phenotypes

It has already been reported by Medioni et al. (2014) that *imp* mutants could either present a conserved main axon length or an aberrant one, with a 50% of occurrence each. We corroborate this results by applying the k-means automatic algorithm which separated our Imp population in Imp L and Imp Sh, with a 46 vs. 54% of incidence each. This bimodal behaviour can also be seen in the length distribution Figure 5. Surprisingly, we have found other relevant morphological differences between this two groups that have not been yet reported in the bibliography. The main one is the branching points distribution, as Imp Sh is significantly more densely branched than Imp L (Table 3 and Table 4). Also, the percentage of branches ranging from 1 to 5 µm, while aberrant in Imp L, is conserved in Imp Sh (which shows no differences from WT (Table 6)).

Regarding the general likelihood analysis (Table 8), while less than 20% of Imp Sh neurons can be considered to have a WT phenotype, 55% of Imp L do, allowing to conclude that Imp L presents a generally more wild type phenotype. Finally, we can conclude that the penetrance of the phenotype is ~63%, following our general likelihood analysis (Table 13 and Table 14).

5.4 Adding back Profilin rescues the main axon length and the branch length distribution

The general likelihood analysis (Table 13) considering Imp altogether shows that Profilin decreases the percentage of *imp* mutant phenotype from 63 to 40%.

Regarding the main axon length, while the aberrant neurons represent the 54% of the Imp population, they are reduced to only 33% in Prof Rescue (in Prof Rescue 67% of neurons present a conserved length (WT + Imp L) and only 33% do not). Following the branch length distribution resemblance analysis, 33% of Prof Rescue neurons are classified as WT and represent the second maximum percentage after WT itself (only 18 and 15% correspond to Imp L and Sh, respectively). Looking at the *p* values between branch length categories (Table 6 and Table 7), we can conclude that Profilin rescues the late pruning showing a conserved percentage of L_2 branches and also allows to develop long branches. Even though the percentage of branches in L_4 is slightly smaller for Prof Rescue than WT (Table 5), this difference does not come out as significant in the statistical tests, suggesting a conserved percentage of long branches in Prof Rescue which is not seen in Imp Sh nor in Imp L.

Finally, regarding the general likelihood analysis considering Imp L and Imp Sh separately (Table 14), we conclude that Profilin rescue diminishes the general morphological aberration, as it moves the tendency towards WT and Imp L phenotypes and diminishing the percentage of neurons with an Imp Sh phenotype.

6 CONCLUSIONS

In this work we proposed probabilistic models describing the behaviour of relevant morphological features (i.e. main axon length and shape as well as branch length and density) in Drosophila gamma neurons. This approach allows to accurately describe as well as differentiate genetically different Drosophila gamma neurons considering their morphology. The similarities and differences we are able to enunciate thanks to this work between wild type neurons and the studied mutants directly help to the understanding of the role of Imp and Profilin during axonal remodelling, particularly on axon elongation and branch formation.

We propose that this method consisting in feature selection, model application and likelihood analysis could be applied to any case of study between species where similarities are as important as differences. We can also conclude that the study of individuals is relevant and more enriching than just population analysis driven by ordinary statistics.

ACKNOWLEDGEMENTS

This work was supported by the French Government (National Research Agency, ANR) through the « Investments for the Future » LABEX SIGNALIFE: program reference # ANR-11-LABX-0028-01.
All the authors are within Morpheme (a joint team between Inria CRI-SAM, I3S and IBV).

REFERENCES

Forbes, C., Evans, M., Hastings, N., and Peacock, B., 2011. *Statistical distributions*, John Wiley & Sons, 4th edition.

Guerra, L., McGarry, L. M., Robles, V., Bielza, C., Larranaga, P., & Yuste, R., 2011. Comparison between supervised and unsupervised classifications of neuronal cell types: a case study. *Developmental neurobiology*, *71*(1), 71-82.

Keller, M.T. and Trotter, W.T., 2015. *Applied Combinatorics*. Georgia Institute of Technology, Preliminary Edition.

Kemeny, J. G., and Snell, J. L., 1960. *Finite markov chains*, vol. 356. van Nostrand, 1st edition.

Kong, J. H., Fish, D. R., Rockhill, R. L., and Masland, R. H., 2005. Diversity of ganglion cells in the mouse retina: unsupervised morphological classification and its limits. *J. of Comp. Neurology*, *489*(3), 293-310.

López-Cruz, P. L., Larrañaga, P., DeFelipe, J., and Bielza, C., 2014. Bayesian network modeling of the consensus between experts: An application to neuron classification. *Int. J. of Approx. Reasoning*, *55*(1), 3-22.

Luo, L., 2002. Actin cytoskeleton regulation in neuronal morphogenesis and structural plasticity. *Annual review of cell and developmental biology*, *18*(1), 601-635.

Medioni, C., Ramialison, M., Ephrussi, A., and Besse, F., 2014. Imp promotes axonal remodeling by regulating profilin mRNA during brain development. *Current Biology*, *24*(7), 793-800.

Mottini, A., Descombes, X., and Besse, F., 2013. Tree-like shapes distance using the elastic shape analysis framework. In *British Machine Vision Conference*.

Mottini, A., Descombes, X., Besse, F., and Pechersky, E., 2014. Discrete stochastic model for the generation of axonal trees. In *EMBS*, 6814-6817.

Mottini A, Descombes X., and Besse F., 2014. From Curves to Trees: A Tree-like Shapes Distance Using the Elastic Shape Analysis Framework. *Neuroinformatics*, 13, 175–191.

Myatt, D. R., Hadlington, T., Ascoli, G. A., and Nasuto, S. J., 2012. Neuromantic–from semi-manual to semi-automatic reconstruction of neuron morphology. *Frontiers in neuroinformatics*, *6*.

Redt-Clouet, C et al., 2012. Mushroom body neuronal remodelling is necessary for short-term but not for long-term courtship memory in Drosophila. *European Journal of Neuroscience*, *35*(11), 1684-1691.

Schindelin, J et al, 2012. Fiji: an open-source platform for biological-image analysis. *Nature meth.9*(7), 676-682.

Schlüter, K., Jockusch, B. M., and Rothkegel, M., 1997. Profilins as regulators of actin dynamics. *Biochimica et Biophysica Acta (BBA)-Molecular Cell Research*, *1359*(2), 97-109.

Szebenyi, G., Callaway, J. L., Dent, E. W., and Kalil, K., 1998. Interstitial branches develop from active regions of the axon demarcated by the primary growth cone during pausing behaviours. *The Journal of neuroscience*, *18*(19), 7930-7940.

Tessier, C. R., and Broadie, K., 2008. Drosophila fragile X mental retardation protein developmentally regulates activity-dependent axon pruning. *Development*, *135*(8), 1547-1557.

Verheyen, E. M., and Cooley, L., 1994. Profilin mutations disrupt multiple actin-dependent processes during Drosophila development. *Development*, *120*(4), 717-728.

Williams, D. W., and Truman, J. W., 2005. Remodeling dendrites during insect metamorphosis. *Journal of neurobiology*, *64*(1), 24-33.

Wu, J. S., and Luo, L., 2006. A protocol for mosaic analysis with a repressible cell marker (MARCM) in Drosophila. *Nature protocols*, *1*(6), 2583-2589.

Xie, Z., Huang, C., Ci, B., Wang, L., and Zhong, Y., 2013. Requirement of the combination of mushroom body γ lobe and α/β lobes for the retrieval of both aversive and appetitive early memories in Drosophila. *Learning & Memory*,*20*(9), 474-481.